Rectification and Rapid Activation at Low Ca^{2+} of Ca^{2+}-Activated, Voltage-Dependent BK Currents: Consequences of Rapid Inactivation by a Novel β Subunit

Xiao-Ming Xia, Jiu-Ping Ding, Xu-Hui Zeng, Kai-Lai Duan, and Christopher J. Lingle

Washington University School of Medicine, Departments of Anesthesiology, and Anatomy and Neurobiology, St. Louis, Missouri 63110

A family of accessory β subunits significantly contributes to the functional diversity of large-conductance, Ca^{2+}- and voltage-dependent potassium (BK) channels in native cells. Here we describe the functional properties of one variant of the β subunit family, which confers properties on BK channels totally unlike any that have as yet been observed. Coexpression of this subunit (termed β3) with *Slo* α subunits results in rectifying outward currents and, at more positive potentials, rapidly inactivating ($\sim$1 msec) currents. The underlying rapid inactivation process results in an increase in the apparent activation rate of macroscopic currents, which is coupled with a shift in the activation range of the currents at low Ca^{2+}. As a consequence, the currents exhibit more rapid activation at low Ca^{2+} relative to any other BK channel subunit combinations that have been examined. In part because of the rapid inactivation process, single channel openings are exceedingly brief. Although variance analysis suggests a conductance in excess of 160 pS, fully resolved single channel openings are not observed. The inactivation process results from a cytosolic N-terminal domain of the β3 subunit, whereas an extended C-terminal domain does not participate in the inactivation process. Thus, the β3 subunit appears to use a rapid inactivation mechanism to produce a current with a relatively rapid apparent activation time course at low Ca^{2+}. The β3 subunit is a compelling example of how the β subunit family can finely tune the gating properties of Ca^{2+}- and voltage-dependent BK channels.

Key words: accessory subunits; K$^+$ channels; BK channels; Ca^{2+}- and voltage-gated K$^+$ channels; mSlo channels; inactivation

Ca^{2+}- and voltage-dependent K$^+$ (BK-type) channels, like the voltage-gated K$^+$ channels, are composed of four homologous α subunit peptides that contribute to the ion channel pore (Atkinson et al., 1991; Adelman et al., 1992; Butler et al., 1993; Shen et al., 1994), along with β accessory subunits that regulate many important aspects of BK channel function (McManus et al., 1995; Wallner et al., 1995, 1999; Dworetzky et al., 1996; Tseng-Crank et al., 1996; Nimigean and Magleby, 1999; Xia et al., 1999). Typically, BK channels exhibit a stereotypic, large unitary conductance but exhibit considerable functional diversity in regards to kinetic behavior, apparent Ca^{2+} dependence, and pharmacology (McManus, 1991). Thus, BK channels can play a variety of physiological roles well suited to the demands of the cells in which they are found. The functional diversity can, in part, be accounted for by various splice variants of the α subunit encoded by the *Slo* loci (Adelman et al., 1992; Tseng-Crank et al., 1994; Jones et al., 1998; Ramanathan et al., 1999). However, the family of accessory β subunits may, in fact, play a more important role in defining the phenotypic properties of BK channels, including the effective gating range and inactivation behavior (McManus et al., 1995;

Jones et al., 1998; Wallner et al., 1999; Xia et al., 1999), because the functional variation arising from *Slo* splice variants appears rather modest (Adelman et al., 1992; Tseng-Crank et al., 1994; Saito et al., 1997; Jones et al., 1998; Ramanathan et al., 1999). To date, including the subunit studied in this paper, four distinct members of a mammalian β subunit family have been identified [KCNMB1 (β1) (Knaus et al., 1994); KCNMB2 (β2) (Wallner et al., 1999; Xia et al., 1999); KCNMB3 (β3) (Riazi et al., 1999; Brenner et al., 2000; Uebele et al., 2000); KCNMB4 (β4) (Wickenden et al., 1999; Brenner et al., 2000; Meera et al., 2000; Wallner et al., 2000)], each of which appears to confer unique functional properties on the resulting BK channels. Definition of the functional properties of the β subunits is an essential step in understanding the diversity of phenotypic properties of BK channels in native cells.

Here, we describe the functional properties of new β subunit (termed β3) that confers onto BK channels properties totally unlike any that have as yet been described. Genomic sequence encoding a portion of this subunit has been described recently (Riazi et al., 1999), although the subunit we have identified contains differences in the N terminus from that proposed. Coexpression of this new subunit with *Slo* α subunits results in an extremely rapidly inactivating, Ca^{2+}- and voltage-dependent current with pharmacological properties characteristic of previously described BK channels. However, the currents have several properties unlike other BK currents, including rectification of outward current and extremely flickery, unresolvable single channel openings. The effects of this particular β subunit family member illustrate an extreme example of the diverse ways ion channel function can be altered by an accessory subunit.

MATERIALS AND METHODS

Identification of the full-length cDNA clone of β3. Using homology searching of human expressed sequenced tagged (EST) databases based on BK β1 (Knaus et al., 1994), an avian β subunit (Oberst et al., 1997), and β2 (Wallner et al., 1999; Xia et al., 1999) sequences, several partial cDNA sequences (GenBank accession numbers AA761761, AA195511, AA823768, and AA236968) suggestive of a new β subunit family member were identified. These cDNA clones were obtained from Genome Systems (St. Louis, MO) and resequenced with BigDye Terminator Kit (Applied Biosystems, Foster City, CA). The four EST cDNA clones exhibited sufficient overlap to define most of the β3 sequence, including the 3′ terminus, but terminated at a position aligning within TM1 defined by the other β subunits. Thus, the EST cDNA clones failed to identify a full-length clone and lacked the start codon at the 5′ end. To search for the 5′ coding sequence, a nested PCR was performed on human heart cDNA library (Stratagene, La Jolla, CA), from which several of the EST clones had been identified. The two rounds of PCR were performed with a vector-specific primer and a β3-specific primer (first PCR, Lacmer and 5′-CATCATGGCAAACCCCAGCATCAC-3′; second PCR, T3 primer and 5′-GAAGATCTCCCAGCATCACGGCTCGGTCCTCTCC-3′, with pfu polymerase, 30–36 cycles, 96°C for 30 sec, 50°C for 45 sec, and 72°C for 2 min). The PCR products were then purified and digested with *Eco*RI and *Bgl*II overnight and then gel purified and subcloned in pSK plasmid (Stratagene). Sequencing revealed that one pSK clone contained an extra 500 base pairs upstream of the β3 sequence. The continuity of this sequence to the rest of β3 was justified by the fact that 46 base pairs at the 3′ end of the PCR-generated fragment were identical to sequence obtained from the partial β3 sequence identified by the EST sequences. This new sequence identified by PCR define 19 additional amino acids at the β3 N terminus that precede an upstream stop codon in the same reading frame.

Tissue distribution of the β3 message. Northern blots were performed on membranes purchased from Clontech (Palo Alto, CA) containing ~2 μg of poly(A$^+$) RNA per lane from various human tissues. The PCR fragment of full-length β3 was ^{32}P-labeled as the hybridization probe. The vendor adjusted the RNA loading of each lane based on previous blots using human β-actin cDNA as probe. The experimental conditions used were described previously (Xia et al., 1999).

Expression constructs. The *Xenopus* oocyte expression vector pBF was used to subclone all of the DNA constructs (Xia et al., 1998). The *mSlo* α subunit [GenBank accession number L16912 (Butler et al., 1993)] was digested with *Cla*I and filled in to generate blunt ends at the 5′ end of *mSlo*; a 3′ *Sal*I site was used to obtain a blunt-*Sal*I fragment. The resultant *mSlo* was then subcloned into a *Hpa*I-*Sal*I-digested pBF vector. The full-length β3 expression clone was generated by overlapping PCR and DNA manipulation. The 3′ part was obtained by subcloning β3 *Eco*RI fragment from EST clone AA761761 to the *Eco*RI-digested vector portion of AA195511, which contains partial β3 3′ end sequence. This intermediate construct, which is a partial β3 sequence lacking the 5′ end, was screened by sequencing to define the correct orientation. The complete full-length β3 clone was then acquired by overlapping PCR (Xia et al., 1999) (first round PCR primer, reaction A, 5′-AGGGATCCAC-TGCCAATGACAGCCTTTCCTG-3′ and 5′-GGCAGCCTCTTGTG-CACATCTAGTGGGTCTCCATC-3′; reaction B, 5′-GATGGAGA-CCCACTAGATGTGCACAAGAGGCTGAA-3′ and 5′-TACTAGTC-GACTTAAGATTTCTCTGCTCTTCCTT-3′; second round PCR primer, 5′-AGGGATCCACTGCCAATGACAGCCTTTCCTG-3′ and 5′-TACTAGTCGACTTAAGATTTCTCTGCTCTTCCTT-3′; pfu polymerase, 30–36 cycles, 96°C for 30 sec, 52°C for 45 sec, and 72°C for 2 min). The final overlapping PCR product was digested with *Bam*HI and *Sal*I and subcloned in the *Bam*HI-*Sal*I pBF oocyte expression vector (Xia et al., 1998). Both strands of DNA were sequenced for verification.

β3 N-terminal or C-terminal deletion constructs D3, D4, and D5 were generated by pfu PCR with specific β3 primers (D3 primer, D4 primer, and D5 primer). The β2 N terminus β3 chimera (construct D1) and β3 N terminus β2 chimera (construct D20) were generated by overlapping PCR (Xia et al., 1999). To study the other potential 5′ alternative hβ3 variant (Riazi et al., 1999), we amplified the 5′ end from HEK293 genomic DNA using pfu PCR and then used overlapping PCR to link the 5′ sequence with the rest of the 3′ hβ3 sequence. In the first round PCR, two PCR reactions were performed using either human genomic DNA (A) or hβ3 DNA (B) as templates (reaction A primers, 5′-ATATATCTAGACA CAGGTAGGCAGCAAATGAGATTATCC-3′ and 5′-GGCAGCCTAT TGTGCACATCTAGTGGGTCTCCATC-3′; reaction B primers, 5′-GATGGAGACCCACTAGATGTGCACAAGAGGCTGCC-3′ and 5′-

CTACGTCGACTTAAGATTTCTCTGCTCTTCCTT-3′; pfu DNA polymerase, 96°C for 30 sec, 50°C for 30 sec, and 72°C for 1 min, 36 cycles). The second round PCR was performed using both reaction A and reaction B as templates (primer, 5′-ATATATCTAGACACAGGTAGGCAG-CAAATGAGATTATCC-3′ and 5′-CTACGTCGACTTAAGATT-TCTCTGCTCTTCCTT-3′; pfu DNA polymerase, 96°C for 30 sec, 50°C for 30 sec, and 72°C for 2 min, 36 cycles). The reaction product was then purified, digested with *Xba*I and *Sal*I overnight, gel-purified, and subcloned into the *Xba*I-*Sal*I pBF vector. Both strands of DNA were sequenced for verification. This molecule is referred to as Gmhβ3.

Expression in Xenopus *oocytes.* Methods of expression in *Xenopus* oocytes were as described previously (Xia et al., 1999). SP6 RNA polymerase was used to synthesize cRNA for oocyte injection after DNA was linearized with *Mlu*I (Xia et al., 1998). Fifty nanoliters of cRNA (10–20 ng/μl) was injected into stage IV *Xenopus* oocytes harvested 1 d before. To ensure a molar excess of β subunits to *Slo* α subunits, we regularly injected α:β at 1:1 or 1:2 ratios by weight.

During electrophysiological recordings, oocytes were maintained in ND96 [(96 mM NaCl, 2.0 mM KCl, 1.8 mM CaCl$_2$, 1.0 mM MgCl$_2$, and 5.0 mM HEPES, pH 7.5) supplemented with sodium pyruvate (2.5 mM), penicillin (100 U/ml), streptomycin (100 μg/ml), and gentamicin 50 μg/ml]. Oocytes were used 1–7 d after injection of cRNA.

Electrophysiology and analysis. Currents were recorded in either inside-out or outside-out patches (Hamill et al., 1981). Patches used for determination of conductance–voltage (*G–V*) relationships contained large numbers of channels and were typically from oocytes maintained for 3–7 d. Generation of ensemble averages of channel openings was done with patches with fewer channels from oocytes maintained for 1–3 d before recording. Currents were typically digitized at 20–100 kHz. Macroscopic records were filtered at 5–20 kHz (Bessel low-pass filter; −3 dB) during digitization. Single channel records were filtered at 10 kHz (Bessel low-pass filter; −3 dB).

During seal formation, oocytes were bathed in ND96. After excision, patches were quickly moved into a flowing 0 Ca^{2+} solution. For inside-out recordings, the pipette extracellular solution was 140 mM potassium methanesulfonate, 20 mM KOH, 10 mM HEPES, and 2 mM MgCl$_2$, pH 7.0. Test solutions bathing the cytoplasmic face of the patch membrane contained 140 mM potassium methanesulfonate, 20 mM KOH, 10 mM HEPES, pH 7.0, and one of the following: 5 mM EGTA (for nominally 0 Ca^{2+}, 0.5 μM, and 1 μM Ca^{2+} solutions), 5 mM HEDTA (for 4 and 10 μM Ca^{2+} solutions), or no added Ca^{2+} buffer (for 60 μM, 100 μM, 300 μM, and 5 mM Ca^{2+} solutions). The methanesulfonate solutions were calibrated to be identical to a set of chloride-containing solutions with free Ca^{2+} determined from a computer program (EGTAETC; E. McCleskey, Vollum Institute, Portland, OR). Calibration was also performed against a commercial set of Ca^{2+} standards [World Precision Instruments (WPI), Sarasota, FL], which yielded values essentially identical to our Cl$^-$-based standards. In all cases, the desired free Ca^{2+} was obtained by titrating the solution with calcium methanesulfonate until the electrode measurement of the methanesulfonate-based solution matched that of the chloride-based solution and the WPI calibration solution. Local perfusion of membrane patches was as described previously (Solaro and Lingle, 1992; Solaro et al., 1997).

Voltage commands and acquisition of currents was accomplished with pClamp 7.0 or 8.0 for Windows (Axon Instruments, Foster City, CA). Current values were measured using ClampFit (Axon Instruments), converted to conductances, and then fit with a nonlinear least squares fitting program. As described in Results, conductances were determined in three ways: from tail currents, from the peak current at a given activation potential, and from steady-state current at a given activation potential. *G–V* curves for activation were fit with a Boltzmann equation with the form:

$$G(V) = G_{max}/(1 + \exp[(-V + V_{0.5})/k]) \qquad (1)$$

where $V_{0.5}$ is the voltage of half-maximal activation of conductance, and k is the voltage dependence of the activation process (units of millivolts). At room temperature, the net charge (z) moved between closed and open conditions is given by 25.26/k. To evaluate steady-state conductance–voltage relationships, a double Boltzmann that included terms for both activation and block was used:

$$G(V) = G_{max}/(1 + \exp[(-V + V_{0.5})/k] + K_b(0)*\exp(-zFV/RT)) \qquad (2)$$

where $V_{0.5}$ and k correspond to the voltage of half-activation and voltage dependence of activation, respectively, and $K_b(0)$ is the 0 voltage equi-

A


```
                                                                    TM1
β1   1  M--------- ---------- ---------- -VK-KLVMAQ KRGETRALCL GVTMVVCAVI   29
cβ   1  M--------- ---------- ---------- LAK-KLVTAQ KRGETRALCL GLGMVACSMM   30
β2   1  MFIWTSGRTS SSYRHDEKRN IYQKIRDHDL LDKRKTVTAL KAGEDRAILL GLAMMVCSIM   60
β3   1  M--------- -TAFPASGKK RETDYSDGDP LDVHKRLPSS T-GEDRAVML GFAMMGFSVL   49
β4   1  M--------- ---------- ---------- -AKLRVAYEY TEAEDKSTRL GLFLIISGVV   30

        TM1                           C1                              C2
β1  30  TYYILVTTVL PLYQKSVWTQ ESKCHLIETN -IRDQFE-LK GKKVP----- -QYPCL--WV   79
cβ  31  MYFFIGITIV PFYKTKSVWTT ETICKVLKAN -IKDKTH-CT NSEGSEDEDI FHYPCLQVWV   88
β2  61  MYFLLGITLL RSYMQSVWTE ESQCTLLNAS -TTETRN-CS FSCGPDCWKL SQYPCLQVYV  118
β3  50  MFFLLGITIL KPFMLSIQRE ESTCTAIHTD -IMDDWLDCA FTCGVHCGQ GKYPCLQVFV  108
β4  31  SLFIFGFCWL SPALQDLQAT EANCTVLSVQ QIGEVFE-CT FTCGADCRGT SQYPCVQVYV   89

                        ********* C3                     C4
β1  80  VSAAGRWAV LYHTEDTRDQ NQQCSYIPGS VDNYQTARAD VEKVRAKFQE Q---QVFYCF  136
cβ  89  LTASGQEVM LYHTEDTLER NPKCSYVPGN SENSKEVKAR IETNASNFK- K--YQTFPCY  145
β2 119  LTSSGEKL LYHTEETIKI NQKCSYIPKC GKNFEESMSL VNVMENBR- K--YQHFSCY  175
β3 109  LSHPGQKAL LHYNEEAVQI NPKCFYTPKC HQDRNDLENS ALDKEFEDH KNGT-PFSCF  167
β4  90  NSESNSRAL LHSDEHQLLT NPKCSYIPPC KRENQKNLES VMNWQQYWKD EIGSQPFTCY  149

                               TM2
β1 137  SAPRG ETSV LFQRLYGPQA LLFSLFWPTL LLTGGLLIIA MVKSNQYLSI LAAQK      191
cβ 146  YDPGGMQTNV IILSRLYPPKG LLFTFLWPTL MFTGGCLIIV LVKISQYFSV LSARQ      200
β2 176  SDPEGNQKSV ILYKLYSSNV LFHSLFWPTC MMAGGVAIVA MVKLTQYLSL LCERIQRINR  235
β3 168  YSPASQSEDV IILKKYDQMA IFHCLFWPSL TLLGGALIVG MVRLTQHLSL LCEKYSTVVR  227
β4 150  FNQHQRPDDV LLHRTHDEIV LLHCFLWPLV TFVVGVLIVV LTICAKSLAV KAEAMKKRKF  209

β3 228  DEVGGKVPYI EQHQFKLCIM RRSKGRAEKS                                    257
β4 210  S                                                                  210
```

Figure 1. A family of β subunits for the Ca²⁺-dependent, voltage-gated K⁺ channel. *A,* Amino acid alignment of human KCNMB1 β1 (hβ1), quail β (cβ), human KCNMB2 (hβ3), human KCNMB3 (hβ4), and human KCNMB4 (hβ4) subunits. *Highlighted* residues are those with identity to aligned residues in at least one other β subunit. The two predicted transmembrane segments (Knaus et al., 1994) are marked with *lines* both *above* and *below*. Residues known to be involved in CTX binding of hβ1 [amino acids 90–94 of the β1 subunit (Hanner et al., 1997)] are marked with a *row of asterisks*. *B,* 5′ genomic sequence of KCNMB3 starting with proposed start codon ATG (Riazi et al., 1999). The exon sequence is *shaded* with the splicing elements in *bold*. The splicing site is marked by an *arrow*. *C,* Standard example of an exon–intron junction and the elements involved in mRNA splicing. The intron sequence is *italicized*. The 5′ and 3′ splicing sites are marked by *arrows*. The genomic sequence for β3 contains several features characteristic of a consensus splice site, including 12 pyrimidines just upstream of the AG junction (*bold CTCCCTTTCCCC* in *B*), separated by 2–24 nucleotides from an upstream branch site of seven nucleotides. The *subscripts* indicate the percent occurrence of the specified base (or type of base) at each consensus position. *Py,* Pyrimidines; *Pu,* purines; *N,* any bases. For mRNA splicing, the intron is defined by a GT-AG rule, which corresponds to the 5′ donor and 3′ acceptor. Besides the GT-AG, short consensus sequences are required for the completion of splicing, such as a branch site (*underlined TCTTTAT* in *B*) located ~18–40 nucleotides upstream of the 3′ site (Lewin, 1997).

B

ATGTTCCCCC **TTCTTTAT**GA GCTCACTGCA GTATCTCCTT **CTCCCTTTCC**

CCAA**AGGACA** *GCCTTTCCTG* *CCTCAGGGAA* *GAAGAGAGAG* *ACAGACTACA*
   ^

C

Exon A$_{64}$G$_{73}$ *G$_{100}$U$_{100}$...* *...Py$_{80}$NPy$_{80}$Py$_{87}$Pu$_{75}$APy$_{95}$*...2-24N...12PyNC$_{65}$A$_{100}$G$_{100}$ N Exon
       ^   ^
5' splicing donor   Branch site   3' splicing acceptor

---

librium constant for the blocking reaction, with *z,* the fractional charge moved during the blocking reaction, and *F, R,* and *T* with their usual meanings. This form of a Boltzmann equation can be related to specific molecular steps for simple activation and blocking schemes in which blockade proceeds strictly from open states, i.e., C ⟷ O ⟷ B.

Ensemble averages were generated using our own software. Traces obtained in 0 Ca²⁺ were used to generate an idealized trace that was then subtracted from each record subsequent to averaging of the leak-subtracted records.

Experiments were done at room temperature (21–24°C). All salts and chemicals were obtained from Sigma-Aldrich (St. Louis, MO).

Simulation of currents. Simulation of currents was done with custom software developed in the lab, based on manipulation of Q-matrices (Colquhoun and Hawkes, 1981) for up to 30 state models. For the simulations in Figure 11, the following arbitrary model was used:

$$ C1 \underset{k_{-1}}{\overset{3*k_1}{\rightleftharpoons}} C2 \underset{2*k_{-1}}{\overset{2*k_1}{\rightleftharpoons}} C3 \underset{3*k_{-1}}{\overset{k_1}{\rightleftharpoons}} O \underset{k_r}{\overset{k_f}{\rightleftharpoons}} I \qquad \text{(Scheme I)} $$

with $k_1 = 1000$ sec⁻¹, $k_{-1} = 0.5$ sec⁻¹, $k_f = 5000$ sec⁻¹, and $k_r = 2000$ sec⁻¹. The block and unblock transitions were voltage-independent while the net charge movement associated with each step along the activation pathway was 2.23e, divided between activation and deactivation steps.

RESULTS

Identification of a BK β subunit variant conferring very rapid inactivation on BK channels

From searches of human EST databases, several cDNA clones of the same gene were identified that show high homology with known BK channel β subunits, KCNMB1 (β1) (Knaus et al., 1994), an avian β subunit (Oberst et al., 1997), and KCNMB2 (β3) (Wallner et al., 1999; Xia et al., 1999). The identification and isolation of the full-length cDNA clone of the gene hβ3 was completed through nesting PCR and DNA recombination as described in Materials and Methods. hβ3 shares extensive homol-

ogy with other β subunits (Fig. 1). The coding region of β3 is comprised of 771 base pairs and 257 amino acids. The hβ3 protein shares 24% (62 of 257) identities and 37% (96 of 257) similarities with hβ1 (191 amino acids). For comparison, Figure 1 also includes sequence for an additional human neuronal β subunit, KCNMB4 (β4) (Wickenden et al., 1999; Brenner et al., 2000; Meera et al., 2000; Wallner et al., 2000).

The nomenclature given in Figure 1 follows current general usage as now defined through GenBank. In a previous publication from this lab (Xia et al., 1999), we used the designation β3 for the then unnamed KCNMB2 subunit, because identification of the avian β subunit (Oberst et al., 1997) preceded identification of KCNMB2 (β2). Although the relationship of the avian β subunit to other mammalian β subunits remains to be clarified, the terminology used here follows the GenBank designations for the mammalian β subunit family.

With no signal peptide, the topology analysis suggests that β3 probably shares common structural features with the other β subunits, having two transmembrane domains with both N and C terminals residing intracellularly. The β3 subunit is somewhat unusual in having extended C-terminal sequence. There are two potential N-glycosylation sites (N-X-S/T) in the extracellular loop and one consensus PKC phosphorylation site (Basic$_{1-3}$-X$_{0-2}$-(S*/T*)-X$_{0-2}$-Basic$_{1-3}$) located at the penultimate C-terminal residue. β3 shares with the other β subunits four conserved cysteine residues in the extracellular segment.

In the midst of this work, Riazi et al. (1999) published a partial genomic sequence, which, when combined with information from EST data base searches, allowed them to propose a putative gene for a new BK β subunit (Riazi et al., 1999). This putative gene, termed KCNMB3, is identical with our sequence for the 768 base pairs preceding the 3′ stop codon (256 amino acids) but differs at the 5′ end. The N-terminal amino acid sequence of their putative KCNMB3 is 19 amino acids longer than our β3 beginning from the initial Met. Comparison of their genomic sequence with our cDNA sequence identifies a consensus 3′ splicing site in the genomic sequence just at the point of divergence between the two sequences (Fig. 1A). The splicing site is apparently used to generate an initiation ATG site in our cDNA clone and suggests that this 3′ splicing site may be used as an alternative splicing site to generate multiple splicing variants (Fig. 1B,C) (Uebele et al., 2000).

It should also be mentioned that, during completion of this work, another group has reported recently on the functional properties of the identical KCNBM3 variant described here (Brenner et al., 2000). However, in this other study, the properties of currents when α + β3 were presumably coexpressed exhibited little difference from currents resulting from the α subunit alone, in marked contrast to the major differences described below.

Tissue distribution of hβ3 message

Northern blot analysis was used to assess the distribution of β3 mRNA in various human tissues. β3 message was detected in heart, liver, pancreas, adrenal medulla, adrenal cortex, and stomach. Low-level expression of β3 was also detected in skeletal muscle, kidney, thyroid, testis, and small intestine (Fig. 2). The original blot also suggested faint expression in the brain. To determine whether β3 expression might be stronger in particular brain regions, we therefore tested a panel of 14 different brain samples, but only low-level expression of β3 was observed (results not shown). The detected mRNA products are apparently not homogeneous, either within the same tissue or among different
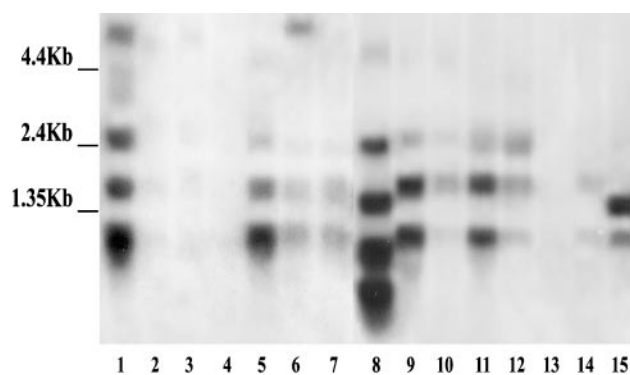
Figure 2. Distribution of β3 message in various tissues. *A*, Northern blots show membranes containing human message probed with radiolabeled human β3 sequence. Tissues are as follows: *1*, heart; *2*, brain; *3*, placenta; *4*, lung; *5*, liver; *6*, skeletal muscle; *7*, kidney; *8*, pancreas; *9*, adrenal medulla; *10*, thyroid; *11*, adrenal cortex; *12*, testis; *13*, thymus; *14*, small intestine; *15*, stomach. The minimal predicted transcript size for the β3 variant described here would be expected to be ∼1 kb.

tissues. In human heart, as many as four products were detected, 1, 1.8, 2.5, and 6 kb, whereas in other tissues, such as liver, adrenal medulla, and adrenal cortex, only two or three products were visible. However, in human pancreas, four products differing from those of heart were detected, 0.5, 0.9, 1.5, and 2.5. Some of these smaller products (0.5 and 0.9 kb) may be the degradation products of the larger ones. In stomach, the major product was 1.5 kb. This diversity in apparent message size, although possibly indicative of degradation, is also consistent with the possible expression of multiple splice variants of the β3 subunit. Based on our sequence, we would expect transcript sizes on the order of at least 1.0 kb, although with no information about noncoding regions, this is only a minimal estimate. Because of the possibility that multiple splice variants may be present in different tissues, these results do not allow us to identify which tissues express the particular N terminal we describe here.

Ca^{2+} and voltage dependence of currents arising from the β3 subunit

The hβ3 message was coexpressed with *Slo* α subunits in *Xenopus* oocytes. Currents obtained from inside-out patches from oocytes expressing hβ3 and α subunits were both voltage- and Ca^{2+}-dependent. Increases in cytosolic Ca^{2+} resulted in shifts in current activation at more negative potentials. In addition, at strong depolarizations and higher Ca^{2+}, α + β3 currents exhibited a very rapid, although incomplete, inactivation (Fig. 3). The time constant of the inactivating portion of current was ∼0.7–1.5 msec (Fig. 4A). The current inactivation time constant exhibits a moderate dependence on membrane voltage (Fig. 4B) and reaches a Ca^{2+}-independent rate at least at the more positive activation potentials (Fig. 4C). Despite the rapid time course of inactivation, inactivation of current is incomplete up to a voltage of +190 mV, and current inactivates to a steady-state level that is dependent on voltage but independent of [Ca^{2+}]. The substantial level of sustained current after inactivation at the most positive activation potentials indicates that both the onset of block and recovery from block that underlie the blocking reaction must be rapid. Furthermore, as will be seen in more detail below, there is a range of voltages and [Ca^{2+}] over which the rapidity of the inactivation is such that current is reduced, despite the fact that no time-dependent inactivation is discernible in the traces. In such cases,
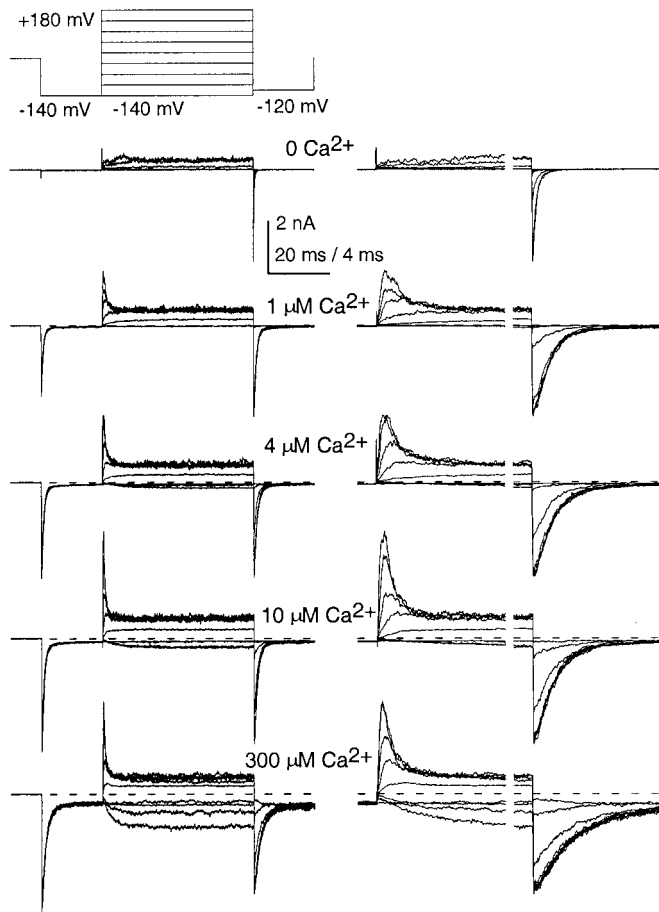
Figure 3. Coexpression of the β3 subunit with the *Slo* α subunit produces rapidly inactivating, Ca²⁺- and voltage-dependent current. *A, Traces* show currents obtained from an inside-out patch from a *Xenopus* oocyte injected with cRNA encoding both human β3 and mouse α subunits. Channels were activated by voltage steps from −140 to +180 mV with 0, 1, 4, 10, and 300 μM Ca²⁺. The voltage protocol is shown at the *top*. *B,* Faster time base records of the currents in *A* are shown for both activation and inactivation and for deactivation. Note that the largest tail current amplitude at −120 mV greatly exceeds the steady-state current level during even the most positive activation steps, indicating that there must be extensive channel unblocking before the peak of the tail current. Also, note that, at 1 and 4 μM Ca²⁺, the maximal tail current at −120 mV is larger than the maximal peak current activated during the voltage step to +180 mV. This suggests that, at lower Ca²⁺, many channels become blocked during the rising phase of outward current.

the current does not appear to be inactivating but does exhibit strong rectification. Another interesting aspect of the currents is that, even at moderate Ca²⁺, e.g., 4 μM, at a potential of +60 and more positive, currents rapidly reach their peak value in ~0.5–2 msec.

To illustrate the unusual features of the β3 currents, Figure 5 compares the properties of currents through channels resulting from the α subunit alone, α + β3, and α + β1, when studied with identical salines and stimulation conditions. Examination of these sets of currents suggests that the β3 subunit, in addition to producing inactivation, shifts the activation range of the resulting channels to more negative potentials at a given Ca²⁺, similar to the β1 subunit. Additionally, the β3 subunit produces a distinct slowing of the deactivation time course at a given Ca²⁺ and voltage, relative to the α subunit alone. However, at Ca²⁺ of 10
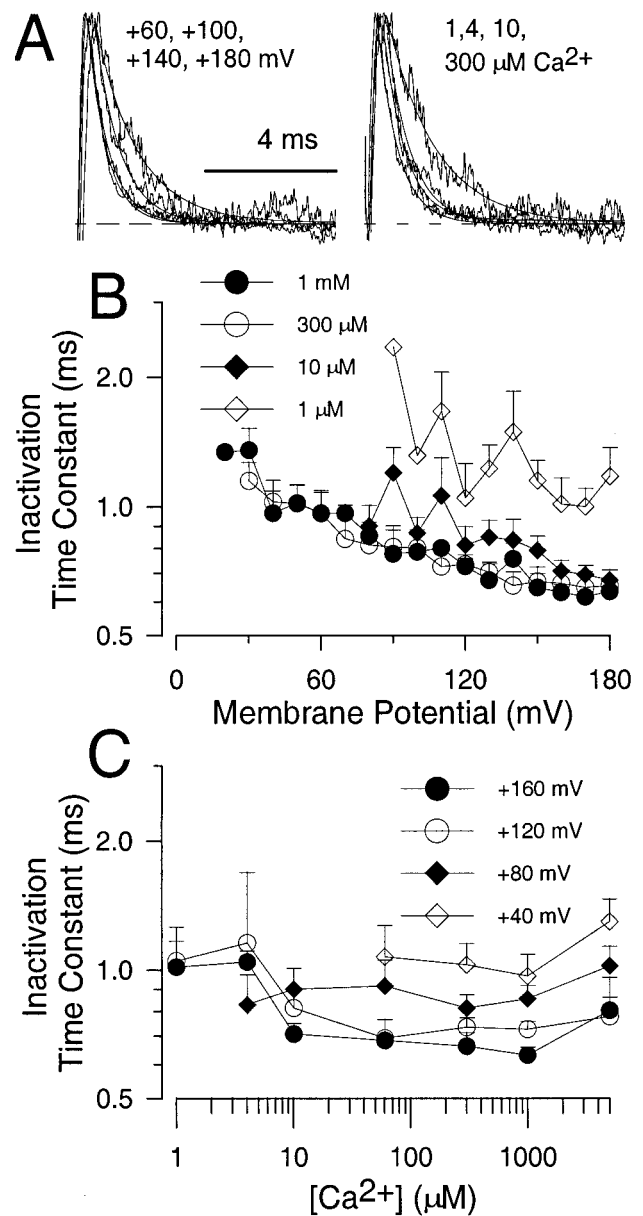
Figure 4. Voltage and Ca²⁺ dependence of the inactivation time constant of β3 currents. *A,* Traces on the *left* show normalized currents (from same patch as Fig. 3) activated with 300 μM Ca²⁺ for +60, +100, +140, and +180 mV. In each case, the best fit of a single exponential function to the current inactivation time course is plotted over the trace, yielding the time constant of inactivation (τ_i). τ_i was 1.26, 0.77, 0.62, and 0.57 msec for +60, +100, +140, and +180 mV, respectively. *Traces* on the right show normalized currents (also from Fig. 3) activated at +140 mV for 1, 4, 10, and 300 μM Ca²⁺. Fitted single exponential functions are also plotted. τ_i was 1.49, 0.74, 0.65, and 0.62 msec for 1, 4, 10, and 300 μM, respectively. *B,* τ_i is plotted as a function of command potential for four different [Ca²⁺]. For each Ca²⁺, there is a small increase in apparent inactivation rate with more depolarized command potential. Each point is the mean ± SEM with four patches for 1 μM Ca²⁺, 10 patches at 10 μM, nine patches at 300 μM Ca²⁺, and five patches for 1 mM Ca²⁺. *C,* τ_i is replotted as a function of [Ca²⁺]. At any voltage, there is little indication of any Ca²⁺ dependence to τ_i at Ca²⁺ of 10 μM and higher.

μM and higher, this slowing of deactivation is less than observed for the β1 subunit. The inactivation mediated by this β3 subunit differs from inactivation for the previously described β2 subunit in several ways (Wallner et al., 1999; Xia et al., 1999). First, β3
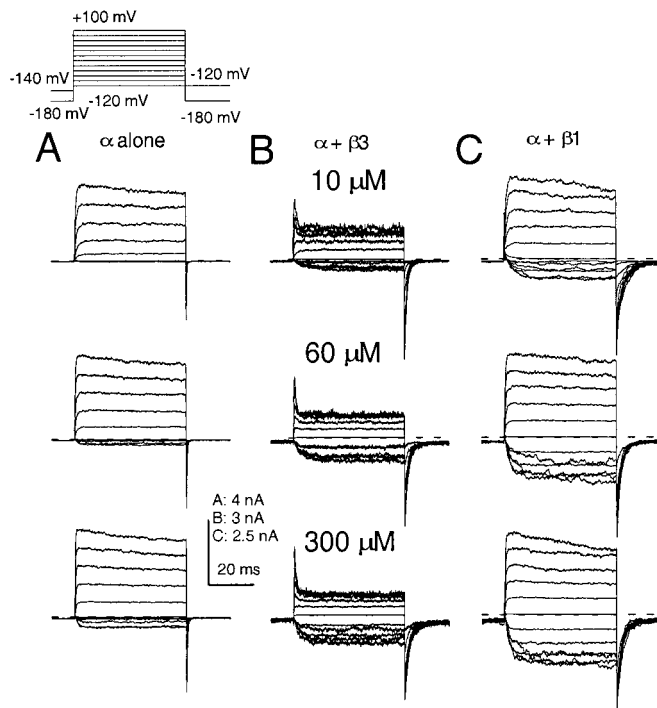
Figure 5. Comparison of currents resulting from α alone, α + β3, and α + β1. *A*, *Traces* show currents resulting from expression of α alone activated by the indicated voltage protocol with 10, 60, and 300 μM Ca^{2+}. *B*, *Traces* show α + β3 currents under the same conditions as in *A*. *C*, *Traces* show currents resulting from α + β1 expression under the same conditions as in *A* and *B*, except that the potential both before and after the activation step was -180 mV. The α + β3 combination results in currents that, at a given Ca^{2+}, are activated at more negative potentials than for α subunits alone but somewhat more positive than for α + β1 subunits. This can be most clearly seen in the tail currents. At 60 μM, the step to -120 mV results in only slight current activation for the β3 construct but produces almost 50% activation for the β1 construct.

inactivation is much more rapid ($\sim$1 vs $\sim$20 msec). Second, there is significant steady-state current during β3 inactivation compared with β2 inactivation. Third, at potentials negative to 0 mV, no time-dependent inactivation is observed for the β3 currents.

In the remainder of this paper, we will focus on qualitative aspects of the currents arising from the β3 subunit, including the macroscopic conductance–voltage behavior, pharmacology, and the appearance of single channel openings. Furthermore, we will present results suggesting that an important functional role of the inactivation process may be to produce Ca^{2+}-dependent K$^+$ current with a relatively fast apparent rate of macroscopic current activation at lower Ca^{2+}.

Properties of conductance–voltage curves arising from coexpression of α + β3 subunits

G–V curves were determined in three separate ways (Fig. 6*A*). First, *G–V* curves were determined from the tail current amplitude after repolarization from various command potentials. Second, conductances were determined from the peak currents measured during each test step. Third, conductances were determined from the steady-state current remaining at the end of each test step.

Visual inspection of the *G–V* curves determined either from the tail currents or the peak currents (Fig. 6*A*) indicates that a similar maximal conductance can be obtained in both cases. This

would seem surprising given the extensive blockade observed in the β3 currents before the repolarizing voltage step. This similarity of the maximal conductance determined from the tail current *G–V* curves to the maximal conductance in the peak current *G–V* curves suggests that most channels that are blocked at the end of the activation step must recover essentially instantaneously during the deactivation step. If this is true, a deactivation step at the peak of outward current should elicit the same tail current amplitude as a deactivation step after a steady-state level of inactivation is achieved. This is, in fact, observed (Fig. 6*B*). Because of this rapid recovery from block, the tail current *G–V* curves therefore appear to provide a direct indication of the fraction of channels activated by a voltage step to different test potentials, despite the extensive inactivation during the test step. It must be kept in mind, however, that the tail current *G–V* curves, in fact, represent not only channels that are open before the deactivation step but also channels that were blocked.

Conductances from tail currents were calculated from a repolarizing step to -120 mV after steps to different activation potentials as shown for one patch in Figure 6*C*. Over all Ca^{2+}, a similar absolute maximal conductance is observed from the tail currents, even with 0 Ca^{2+}. With elevations in Ca^{2+}, the *G–V* curves show the leftward shift characteristic of BK-type channels. In contrast to the tail current *G–V* curve, the steady-state conductance (Fig. 6*D*) exhibits a marked voltage-dependent reduction at more positive potentials, and the absolute amount of steady-state conductance (and current) at all Ca^{2+} from 10 μM and higher is relatively similar at each voltage above 0 mV. Because over these [Ca^{2+}] the tail current *G–V* curves indicate that all channels are essentially maximally activated at any potential above 0 mV (Fig. 6*C*), this indicates that the blocking reaction is essentially Ca^{2+}-independent at 10 μM Ca^{2+} and higher. Even at 1 and 4 μM [Ca^{2+}], at sufficiently high voltages, the steady-state conductance also appears to asymptote to values comparable with those at higher Ca^{2+}. Thus, qualitatively the blocking process appears to be voltage-dependent but primarily independent of Ca^{2+}.

The steady-state conductance was fit in each case with the double Boltzmann given by Equation 2 containing a term for current activation and a second term for a voltage-dependent blocking reaction (Fig. 6*D*). Both the $V_{0.5}$ and k for the activation of conductance were constrained to values obtained from fits to the tail current *G–V* curves shown in Figure 6*C*. The resulting double Boltzmann functions then provided an estimate of the voltage dependence of the blocking reaction with values given in the figure legend. The reduction of conductance at each potential positive to 0 mV was essentially identical for all Ca^{2+} of 10 μM and higher. This is the result expected for a Ca^{2+}-independent, voltage-dependent blocking process in which the channel activation process is maximally activated over this range of conditions. Results from 17 patches studied with [Ca^{2+}] from 10 μM through 5 mM yielded similar conclusions (Table 1).

In the simplest case, Equation 2 arises from the predicted equilibrium condition for a simple three-state model (C $\longleftrightarrow$ O $\longleftrightarrow$ B) in which a voltage-dependent blocking process arises only from open channels. The fitted values for z then provide an indication of the amount of charge movement that occurs during the blocking process. The equivalence of the charge movement during the blocking process over the range of 10 μM to 5 mM Ca^{2+} suggests that, irrespective of the blocking mechanism, the equivalent of a total of $\sim$0.33 elementary charges are moved

Figure 6. The voltage dependence of activation and steady-state properties of inactivation revealed in conductance–voltage curves. *A*, Examples of *G–V* curves obtained from tail current amplitude (*open triangles*), from the peak current (*inverted filled triangles*) measured during the command step, and from the steady-state current at the end of the voltage step (*filled triangles*) are shown for one patch bathed with 300 μM Ca^{2+}. For tail currents, each *point* corresponds to the conductance measured 110 μsec after the nominal imposition of the repolarizing voltage step to −120 mV from a given command potential. Reduction of conductance at the most positive potentials probably reflects some slow cumulative block from contaminating ions. *B*, A repolarizing step to −160 mV was used to compare tail current amplitude and time course either from just after the peak of outward current during a step to +160 mV or after development of the steady-state current level at +160 mV. Despite the fact that the current near the peak is over twofold larger than the steady-state current, the tail current amplitude in each case is essentially identical. τ_d after repolarization near the peak outward current was 0.70 msec, whereas after repolarization from the steady-state current level it as 0.97 msec. *C*, Tail current conductances (from the same patch as in *A*) were determined for 0 (*filled circles*), 0.5 (*open circles*), 1 (*filled diamonds*), 4 (*open diamonds*), 10 (*filled triangles*), and 300 (*open triangles*) μM Ca^{2+}. The *solid lines* are single Boltzmann fits (Eq. 1) to the *G–V* curves. Values were as follows: for 0 μM, $V_{0.5}$ = 113.3 mV, k = 15.3 mV; for 0.5 μM, $V_{0.5}$ = 67.1 mV, k = 15.97; for 1 μM, $V_{0.5}$ = 40.4 mV, k = 15.4 mV; for 4 μM, $V_{0.5}$ = 16.2 mV, k = 15.9 mV; for 10 μM, $V_{0.5}$ = −32.2 mV, k = 16.08; for 300 μM, $V_{0.5}$ = −70.5, k = 17.47 mV. *D*, Steady-state conductances were determined from the average current level at the end of voltage steps to a given activation potential and plotted as a function of command voltage. *Solid lines* are fits of the double Boltzmann function given by Equation 2. Values for $V_{0.5}$ for activation and k for activation were constrained to those obtained in *C*. *E*, Peak conductances were calculated from peak currents at each activation potential using a 0 mV reversal potential and plotted as a function of command potential. The *lines* simply connect the values. *F*, Voltages at which conductance is half-activated are plotted as a

function of [Ca^{2+}] for α alone, α + β1, α + hβ3, and α + β2(Δ33) in which the β2 inactivation has been deleted. Error bars show SD. For α + β3, points at 0, 10, and 300 μM correspond to 17 patches, points at 1, 4, 1000, and 5000 μM correspond to 6–10 patches, and points at 0.5 μM corresponds to three patches. For α alone, each point corresponds to four patches, for α + β1, six patches, and for α + β2(Δ33), at least five patches for each *point*. For graphical purposes, points in nominally 0 Ca^{2+} were plotted at 0.05 μM.
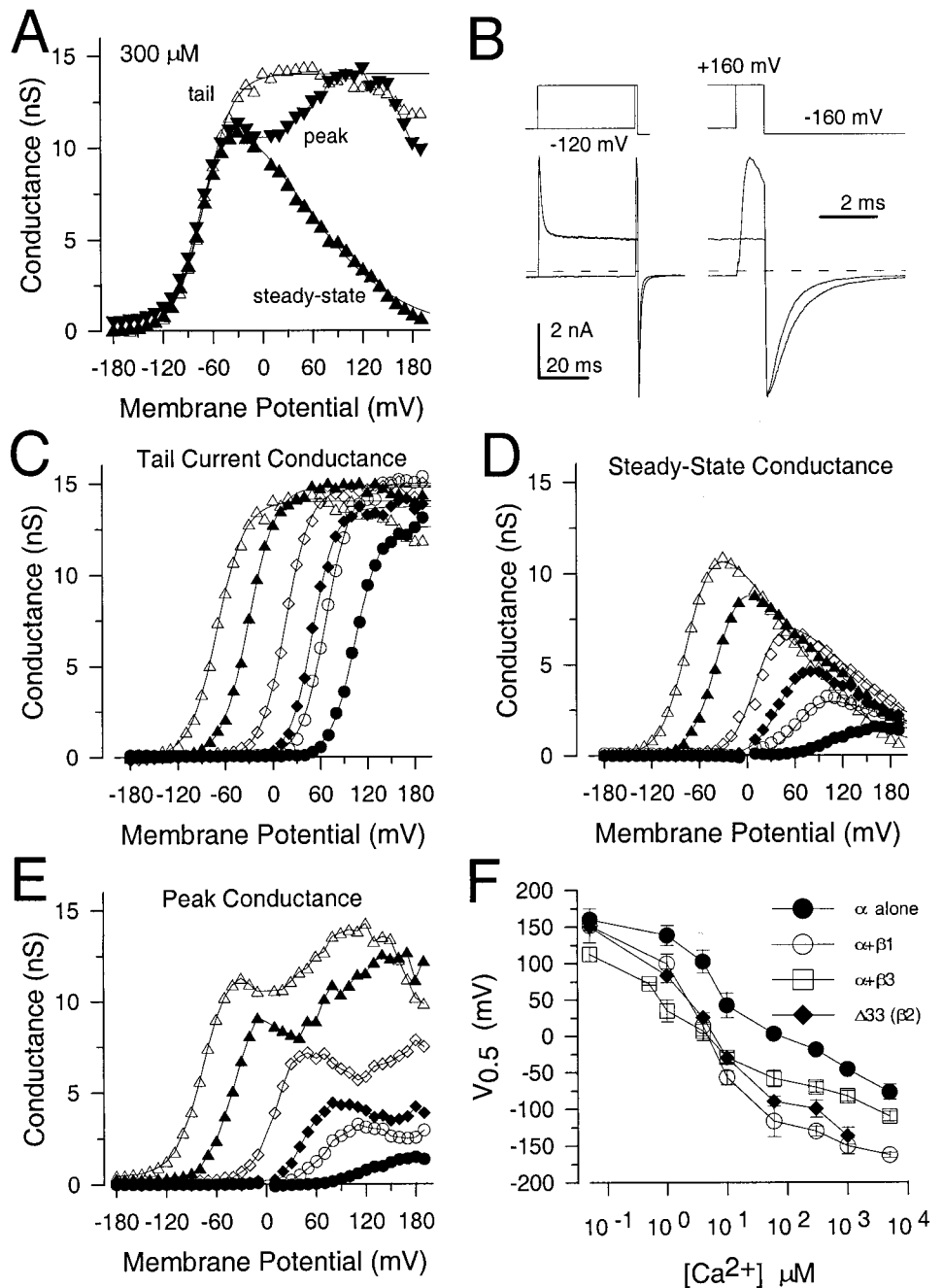
across the membrane in association with the transition(s) from the open to the blocked condition.

When the identical fitting procedure was used to compare tail current and steady-state *G–V* curves at 0, 0.5, 1, and 4 μM Ca^{2+}, Equation 2 was less successful at accounting for the steady-state currents. Specifically, if the values for the blocking reaction at low [Ca^{2+}] were constrained to those obtained from fits to the steady-state *G–V* curves at higher Ca^{2+}, this resulted in large underestimates of the value for maximal conductance at a given Ca^{2+}. If, on the other hand, the maximal value of conductance is con-

strained to be in agreement with the value obtained from fitting the tail current *G–V* curves, the resulting values for $K_b(0)$ for block and the resulting voltage dependence deviate substantially from those obtained at higher Ca^{2+}. Qualitatively, the discrepancy between estimates of the tail current peak conductance and steady-state current peak conductance after accounting for block suggests that, at lower Ca^{2+}, more channels are in blocked states than expected based on the expectations of the simple blocking scheme considered here. A more extensive analysis of the blocking mechanism will be presented elsewhere.

Table 1. Parameters of steady-state block from Equation 2

[Ca^{2+}] (μM)	$K_b(0)$ (mean $\pm$ SD)	z (mean $\pm$ SD)	n (patches)
4	0.353 $\pm$ 0.212	0.33 $\pm$ 0.06	11
10	0.521 $\pm$ 0.148	0.32 $\pm$ 0.03	14
60	0.759 $\pm$ 0.355	0.36 $\pm$ 0.06	8
300	0.579 $\pm$ 0.108	0.42 $\pm$ 0.03	14
1000	0.751 $\pm$ 0.067	0.35 $\pm$ 0.03	5
5000	0.888 $\pm$ 0.088	0.36 $\pm$ 0.04	5

$K_b(0)$, Block association constant at 0 mV; z, fractional charge moved during blocking reaction.

In summary, the voltage-dependent reduction of steady-state current observed with the β3 subunit is consistent with the movement of ~0.33 charges moving across the membrane during the transition from fully open states to blocked states. At high Ca^{2+}, the steady-state features of block are generally consistent with a simple equilibrium between open and blocked states. At low Ca^{2+}, there appears to be more block than might be expected based solely on block of open states alone.

The plot of peak conductance as a function of voltage reveals two other interesting aspects of this current (Fig. 6E). First, at 10 μM Ca^{2+} and above, the peak conductance activated at positive potentials, in general, is similar in most patches to the maximal conductance determined from tail currents, although in some cases the peak conductance never reaches that defined by the tails (Fig. 3). However, for Ca^{2+} well below 10 μM, the maximal conductance activated at positive potentials grossly underestimates the conductance determined from the tail currents. An explanation for this difference is that, at more modest Ca^{2+}, the rapid rate of current inactivation relative to a slower rate of current activation reduces the fraction of channels that are open at any time. Thus, when the underlying activation rates of the current are slow, the rapidity of the inactivation process will simply result in a rectifying current. This will be examined more closely below. Second, the relationship between peak conductance and activation voltage exhibits a novel double hump appearance, which is consistently observed in all patches. Such a behavior can, in fact, be predicted from blocking models in which rates of inactivation are rapid relative to rates of activation over a particular range but for which activation exceeds inactivation rates at more positive potentials (C. J. Lingle, unpublished observations).

Because the inactivated channels do, in fact, recover from inactivation extremely rapidly, the tail G–V curves provide a reasonable indication of the Ca^{2+} and voltage dependence of entry of channels into activated states. For comparison with the β3 subunit, we have also examined patches from oocytes expressing α alone, $\alpha + \beta$1, or $\alpha + \beta$2Δ33 [β2 with the N-terminal inactivation domain removed (Xia et al., 1999,)]. Figure 6F plots the voltage of half-activation as a function of [Ca^{2+}] for all four channel types. The β1 and β2 subunits show the typical marked shift in $V_{0.5}$ relative to α alone with less difference at lower Ca^{2+}. In contrast, $\alpha + \beta$3 produces a marked increase in sensitivity at Ca^{2+} concentrations below 10 μM but produces less of a shift than the β1 subunit at higher Ca^{2+}. These results suggest that the β3 subunit may increase the sensitivity of BK channels to submicromolar or low micromolar Ca^{2+} compared with BK channels modulated by other β subunits. Unlike the β1 and β2 subunits, the β3 subunit appears to shift BK gating at low Ca^{2+} as well as

higher Ca^{2+}, causing a shift of the $V_{0.5}$ versus Ca^{2+} curves, which is somewhat parallel to that obtained with α alone.

In summary, the macroscopic $\alpha + \beta$3 currents exhibit a number of features that may be important in defining their physiological roles. First, the currents appear more sensitive to lower Ca^{2+} than BK channels formed from other known β subunits. Second, the channels exhibit rapid but incomplete inactivation, such that the macroscopic current exhibits a marked steady-state rectification at positive potentials. Third, outward current can be reduced by the inactivation process even when visible, macroscopic inactivation is not observed (for more details, see Fig. 11). A cautionary remark regarding physiological interpretation of these results is that these measurements were all done in symmetrical K$^+$ solutions and at room temperature.

$\alpha + \beta$3 channels exhibit unusual single channel openings

A hallmark of BK channels is a characteristic large single channel conductance. To examine the properties of channels arising from $\alpha + \beta$3 coexpression, we attempted to identify patches with small numbers of channels. An example of a patch from an oocyte expressing $\alpha + \beta$3 subunits is shown in Figure 7. We have been unable to observe single channel openings that are fully resolvable for any such patch studied over a range of Ca^{2+} and activation conditions. Rather, such patches typically exhibit exceedingly brief openings of primarily undefined amplitude, even at a bandwidth of 10 kHz. That such openings do, in fact, represent the behavior of coexpressed $\alpha + \beta$3 subunits is supported by the fact that ensemble averages of such openings reveal the characteristic Ca^{2+} and voltage dependence of activation and the rapid but incomplete inactivation of the macroscopic currents (Fig. 7). Furthermore, ensemble variance analysis suggests a single channel conductance in excess of 150 pS at positive activation voltages (data not shown). Because of the rapid flickering behavior of these openings, this value most certainly underestimates the true channel current. This rapid flickering behavior is, in part, consistent with a rapid inactivation process of ~0.5–1.0 msec. However, the failure to resolve any channel openings that approach the expected single channel current level for α subunits alone suggests that other kinetic factors besides the rapid inactivation may contribute to the unusual flickery behavior of the single channels. To date, we have not been successful in identifying a patch with only a single $\alpha + \beta$3 channel.

Pharmacological properties of the $\alpha + \beta$3 channels

In addition to the characteristic shifts in gating with increases in Ca^{2+}, BK-type channels exhibit specific pharmacological properties. Because of the unusual properties of the currents resulting from $\alpha + \beta$3 coexpression, we examined the pharmacological sensitivity of these currents to various compounds. Extracellular 5 mM 4-aminopyridine was without effect on $\alpha + \beta$3 currents. BK currents are typically blocked by extracellular application of tetraethylammonium (TEA) at concentrations less than those affecting other voltage-dependent K$^+$ channels. The effect of extracellular TEA on either α alone (Fig. 8A) or $\alpha + \beta$3 currents (Fig. 8B) was therefore examined. TEA blocked $\alpha + \beta$3 currents with an IC$_{50}$ of 0.59 $\pm$ 0.30 mM at +100 mV (Fig. 8C) compared with an IC$_{50}$ of 0.43 $\pm$ 0.05 mM for block of α alone. Over the range of +20 to +100 mV, the voltage dependence and fitted value for dissociation constant at 0 mV (for values, see legend to Fig. 8D) were similar between the two currents (Fig. 8D).

Figure 7. Channel openings resulting from co-expression of α + β3 and exhibiting unusual gating behavior. *Traces* in each *column* show channel openings in an inside-out patch bathed with 0, 10, 60, or 300 μM Ca^{2+}, respectively, from *left* to *right*. Channel openings were activated by steps to +100 mV (with the voltage protocol shown on the *top* of the *first column*). Four consecutive sweeps are shown *below* each condition. The *dotted line* indicates a 25 pA current level (250 pS at this voltage). The records were filtered at 10 kHz, and currents were sampled at 100 kHz. *Traces* on the *bottom* of each *column* show ensemble averages for each condition shown *above*. In each case, at least 60 sweeps were included in each average. Averages exhibit the rapid but incompletely inactivating current seen for the macroscopic currents, despite the fact that no fully resolved channel openings are seen. Single exponential fits to the inactivation time course of the averaged currents yielded values of 0.99, 1.37, and 1.18 msec for 10, 60, and 300 μM Ca^{2+}, respectively, comparable with the inactivation time constants of macroscopic currents. Calibration: 30 pA applies to the individual current sweeps, whereas 15 pA applies to the averaged currents.
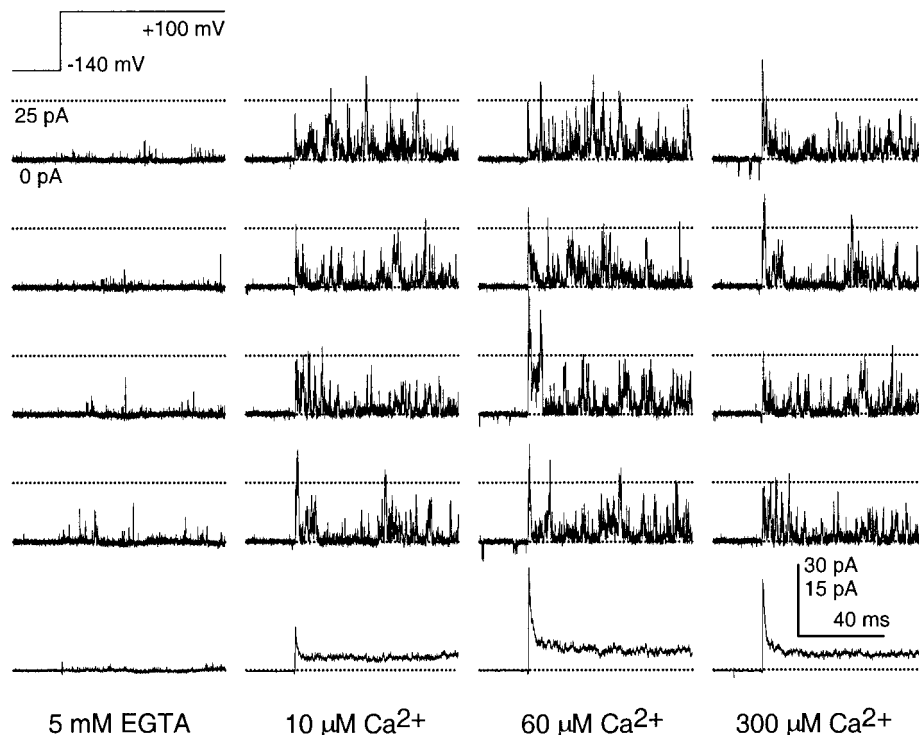
Extracellular charybdotoxin (CTX) inhibited α + β3 currents with an IC$_{50}$ of 80.0 ± 10 nM (*n* = 4) as estimated from the time course of the onset and recovery from CTX blockade at 100 nM (Saito et al., 1997; Xia et al., 1999), assuming that 100% block is defined by 30 mM TEA. This sensitivity of the β3 subunit appears similar to that of the β2 subunit, which is less than for either α + β1 or α alone (Wallner et al., 1999; Xia et al., 1999).

Thus, currents arising from coexpression of α + β3 exhibit pharmacological features characteristic of BK-type channels.

Inactivation results from the β3 N terminus but not the C terminus

Inactivation mediated by the β2 subunit requires an N-terminal structure. Compared with the β2 subunit, the β3 subunit contains a somewhat shorter N terminus but also an extended C terminus that is predicted to be cytosolic. We therefore wished to determine whether either the N- or C-terminal sequences might play a role in inactivation mediated by the β3 subunits. Removal of most of the C terminus of the β3 subunit (construct D3; *n* > 10 patches) had no discernible affect on the ability of β3 subunits to produce inactivating currents when coexpressed with α (Fig. 9*A*). In contrast, removal of the N terminus (construct D4; *n* = 4 patches) resulted in complete removal of inactivation (Fig. 9*B*).

We also examined constructs in which the β2 N terminus and β3 N terminus were swapped between the parent subunits. Replacing the β2 N terminus with a β3 N terminus (construct D20; *n* > 10 patches) resulted in currents with the characteristic rapid but incomplete inactivation of the full-length β3 subunit (Fig. 9*C*). In contrast, when the β3 N terminus is replaced with the β2 N terminus (construct D1; *n* = 4 patches; data not shown), relatively complete inactivation with a time constant of 20–25 msec was observed, characteristic of the full-length β2 subunit.

Finally, we have also examined the functional properties of the previously reported putatively genomic KCNMB3 alternative N-terminal variant (Riazi et al., 1999). The alternative N-terminal variant (construct Gmhβ3) also results in inactivating

BK currents (*n* = 4 patches) (Fig. 9*D*), although inactivation proceeds substantially more slowly (τ$_i$ of ~50 msec).

BK channel blockers do not compete with the inactivation process

Inactivation of BK channels mediated by the β2 subunit N terminus contrasts with N-terminal-mediated inactivation of voltage-dependent K$^+$ channels (Choi et al., 1991) in that cytosolic channel blockers do not slow the rate of current inactivation (Solaro et al., 1997; Xia et al., 1999), suggesting that the inactivation domain of the β2 subunit does not bind directly to sites at the ion channel mouth occupied by the blockers. We did a similar test on inactivation of BK channels mediated by the β3 N terminus, using the rapid cytosolic blocker TEA (Fig. 10). For a simple competition between blocker and any inactivation domain, 50% reduction of peak current amplitude is expected to result in a twofold prolongation of the inactivation time constant (Choi et al., 1991). Over a range of TEA concentrations producing up to a greater than 50% block of peak current, no prolongation of inactivation time course was observed. Similar, to blockade mediated by the β2 N terminus, TEA does not alter the rate of onset of the block process mediated by the β3 N terminus.

Physiological consequences of the rapid blocking process: an increase in apparent current activation rate at low Ca^{2+} and rectification

As indicated earlier, the time constant of β3-mediated inactivation exhibits only a small dependence on voltage or Ca^{2+}; over a range of potentials and Ca^{2+}, inactivation occurs with a time constant of ~0.7–1.5 msec. This rate of current inactivation is rapid relative to the expected rates of BK current activation at moderate [Ca^{2+}] and depolarization. Thus, the modest Ca^{2+} and voltage dependence of the macroscopic τ$_i$ suggests that, at potentials at which activation of current is slow, the kinetics of rapid block may contribute to the time course of apparent current activation. Specifically, if rates of equilibration between open
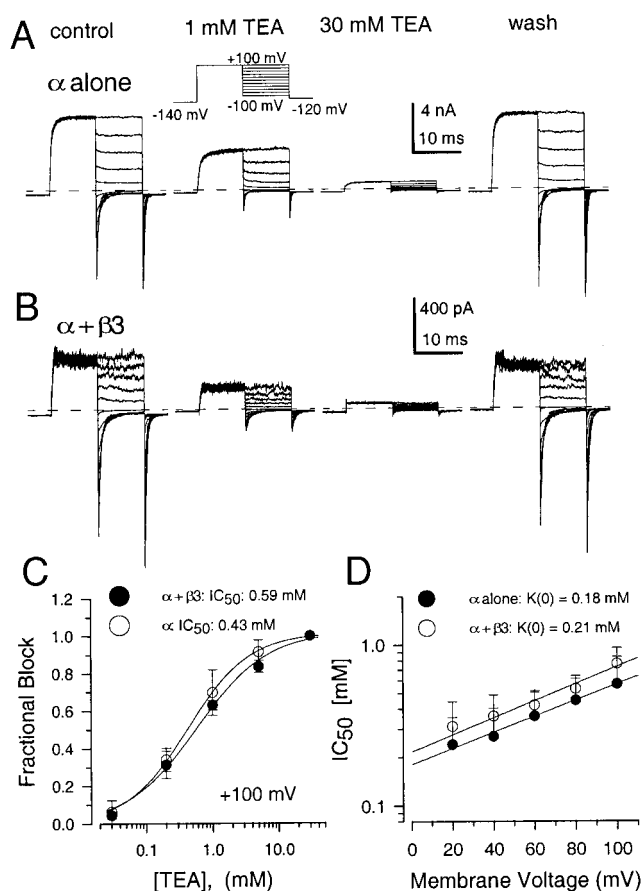
Figure 8. β3 currents exhibit sensitivity to TEA characteristic of other BK currents. *A,* Traces show currents activated by the indicated voltage-protocol (activation steps from −100 to +100 mV) from an outside-out patch from an oocyte expressing the *Slo* α subunit alone with 10 μM Ca^{2+} in the recording pipette. *Left panel* shows currents in control saline, *middle panels* show the effects of 1 and 30 mM TEA applied to the extracellular face of the membrane, and the *right panel* shows currents after removal of TEA. *B,* Traces show currents activated with the same protocol used in *A* from an outside-out patch expressing α + β3 subunits. *C,* The fractional block of current elicited at +100 mV is plotted as a function of extracellular TEA concentration for both α alone (*open circles*) and α + β3 (*filled circles*). Fractional block was normalized to the amount of block produced by 30 mM TEA. The IC$_{50}$ values for block were 0.43 ± 0.05 mM ($n = 3$) for α with a Hill coefficient of 0.82, and 0.59 ± 0.30 mM ($n = 4$) for block of α + hβ3 with a Hill coefficient of 0.94. *D,* Estimates of the IC$_{50}$ for block by TEA are plotted as a function of voltage. Fractional block in each case was measured from the steady-state currents at +20 through +100 mV. *Solid lines* are fits of the function $K(V) = K(0) * \exp(-zFV/RT)$, where $K(0)$ indicates the IC$_{50}$ for block by TEA at 0 mV, F, R, and T have their usual meanings, and z is the fitted value for fractional charge moved during the blocking reaction. For α, $K(0) = 0.18 ± 0.01$ mM with $z = 0.28 ± 0.025$, whereas for α + β3, $K(0) = 0.22 ± 0.04$ mM, with $z = 0.30 ± 0.076$.

states and inactivated states are rapid relative to movement of closed channels to open states, the relaxation of current activation can be strongly determined by the kinetics of the equilibration between open and inactivated. The ability of a rapid blocking process to increase an apparent activation rate may seem somewhat unexpected at first glance. However, this situation is simulated for an arbitrary simple current activation scheme (Scheme I) in Figure 11*A* in which, although the underlying molecular rates of channel activation are identical, the presence of a rapid inactivation decreases the apparent activation time constant and decreases the time-to-peak.
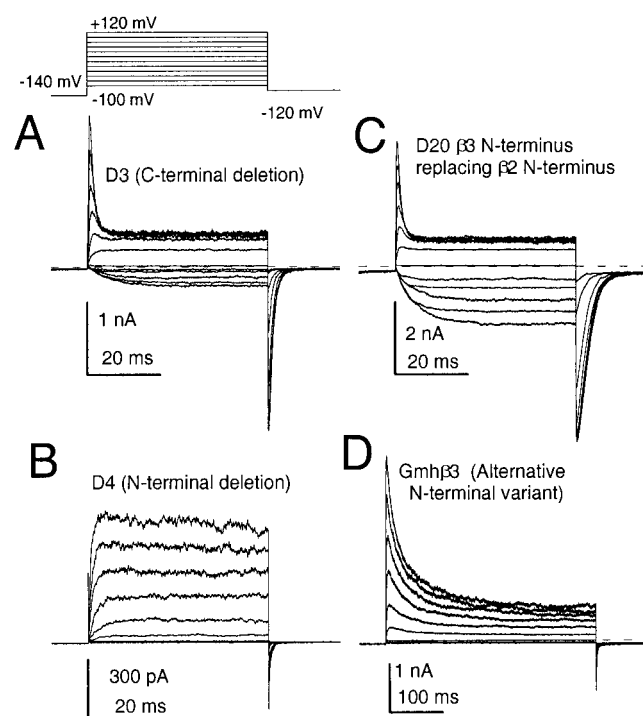

Figure 9. The β3 N terminus, but not the C terminus, is responsible for inactivation of the α + β3 currents. *A,* Thirty-five amino acids from the C terminus of the β3 subunit (construct D3) were removed, and the resulting construct was coexpressed with α subunits. Currents retain the typical inactivation behavior of the intact β3 subunit. Currents were activated with the indicated voltage protocol with 10 μM cytosolic Ca^{2+}. *B,* Twenty-one amino acids were removed from the N terminus of the β3 subunit (construct D4), resulting in loss of the inactivation behavior (10 μM Ca^{2+}). *C,* Twenty-one amino acids from the β3 N terminus were used to replace 33 amino acids at the N terminus of the β2 subunit (construct D20). The D20 construct exhibits the rapid, incomplete inactivation of the β3 subunit but the more negative activation range of the β2 subunit. Currents were activated with 10 μM Ca^{2+}. *D,* The Gmhβ3 alternative splice variant (Riazi et al., 1999) was expressed, and currents were activated with 10 μM Ca^{2+}. Note the different time base for currents in *D*. The time constant of inactivation for this construct at 10 μM and +100 mV was ~50 msec, although the time course of decay is somewhat better described with two exponential components.

To demonstrate this for α + β3 currents, currents were activated in the presence of 10 μM Ca^{2+} at +80 (Fig. 11*B*) and +60 (Fig. 11*C*) mV and tail currents determined at various times of the depolarizing activation step. Qualitatively, in both cases the rate of increase in tail current amplitude as a function of command step duration is slower than the apparent rate of current activation during the activation step itself. The increase in tail current amplitude reflects the rate of channels appearing in open and blocked states and thus represents the net movement of channels into the open state(s). On the other hand, the outward current observed during the activation step represents only channels currently in open states. The *right panels* of Figure 11, *B* and *C*, compare the normalized onset of outward current with the time course of activation defined by the tail currents. The observed rate of outward current activation is 1.5- to 3-fold than that determined from the increase in tail current amplitude.

The time constants of activation defined by the increase in tail current amplitude correspond closely with values for *mSlo* current activation as a function of [Ca^{2+}] defined in other work (Cui et
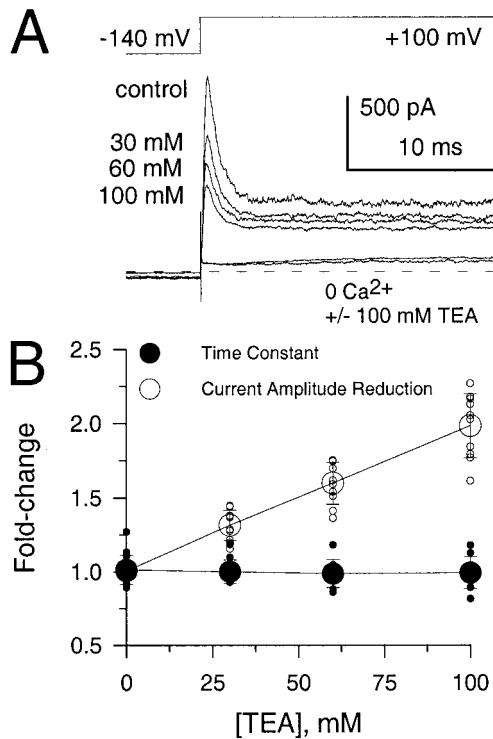
Figure 10. Cytosolic application of TEA does not compete with the native β3 inactivation process. *A*, *Traces* show β3 currents activated by the indicated voltage step with 300 μM cytosolic Ca^{2+} and 0, 30, 60, or 100 mM TEA. A trace was also recorded in 0 Ca^{2+} with 100 mM added TEA. TEA results in a concentration-dependent reduction of peak and steady-state outward current but no effect on the time constant of inactivation. *B*, The fold increase of τ_i by TEA and fold decrease in peak current amplitude is plotted as a function of TEA. For a simple competition between TEA and the inactivation mechanism, both relationships should increase with [TEA] in an identical manner. *Larger symbols* are means with SDs for estimates from five patches. The *smaller symbols* represent individual determinations from these five patches.

al., 1997). Specifically, the value of 1.77 msec for the activation time constant given in Figure 11*B* corresponds well with that expected for 10 μM Ca^{2+} at +60 mV. An apparent activation time constant of 0.66 msec as observed for the rise time of outward in Figure 11*B* would require an effective increase in $[Ca^{2+}]$ at +60 mV in excess of 100 μM (Cui et al., 1997, their Eq. 3).

It should also be noted that, although in some cases there is no visible inactivation during the command step, the steady-state level of current in each case exhibits marked rectification because of rapid block that occurs during the rising phase of current activation. Thus, rapid block confers on these channels two unique characteristics. First, it increases the observed rate of macroscopic current activation at moderate Ca^{2+} compared with channels that lack rapid block. Second, it results in rectification of current.

DISCUSSION

We have described the functional properties of a new member of the BK β accessory subunit family, which confers a number of unique and potentially physiologically important characteristics on the resulting BK channels. First, compared with the β1 and β2 subunits (Wallner et al., 1999; Xia et al., 1999), the $V_{0.5}$ for

activation of this β3 variant is shifted to more negative voltages at lower concentrations of Ca^{2+} (below 10 μM), whereas at higher concentrations of Ca^{2+}, the $V_{0.5}$ is less shifted. Second, the β3 subunit confers an extremely rapid but incomplete blockade of the resulting BK channels. Third, the rapidity of the blocking process is such that it plays a primary role in defining the apparent macroscopic activation kinetics of current and its rectification properties over some activation conditions. Fourth, because of rapid flickering behavior, the properties of single channels containing β3 subunits are unlike any known BK channel. The properties of these currents suggest that, compared with other BK channel variants, they are likely to be more rapidly activated at lower Ca^{2+}. It will be important to determine the properties of this channel under more physiological ionic conditions.

The properties of this β3 subunit variant add significantly to the diversity of functional properties conferred on BK channels by the β subunit family. In fact, β subunits may play the critical role in defining the tissue-specific phenotypic properties of BK channels in various cells. Examination of Northern blots from the β subunits so far examined suggests that there is some tissue overlap among various β subunits. For example, from our work it is clear that both the β2 and β3 variants are expressed in the adrenal medulla (Xia et al., 1999; this study). If different β subunits are expressed in the same cells and, as is likely, assemble into the same single channels, this will add enormously to the variation in BK channel phenotypes, providing cells with an even greater capacity to precisely tune the gating range of the mature BK channels.

Where are channels containing the β3 subunit found?

The channel openings and macroscopic currents resulting from α + β3 subunits exhibit the Ca^{2+} and voltage dependence characteristic of BK channels. Yet, both the unusual single channel properties and the rapid inactivation and rectification appear unique among Ca^{2+}- and voltage-dependent K^+ currents so far described. An intriguing issue then is why has such a current not yet been observed in any native cell. This could arise from a number of reasons. First, in patches with few channels, the flickery behavior of the channels might be difficult to recognize as valid channels. Second, the strongly rectifying behavior of the macroscopic currents means that in a whole-cell recording such a current might be only a minor contributor to the overall outward current. Third, it is possible that this subunit is only expressed in cell types that have not as yet been extensively studied. Although message encoding this subunit family was found in adrenal gland, heart, lung, and kidney, and, to some extent, in the nervous system, the Northern blots provide no information about the distribution of the particular variant we have studied electrophysiologically. A final possibility is that, although message for this variant is found in mRNA, this particular variant is never actually expressed. However, we consider it likely that the restricted expression of some subunits for BK channels may result in a variety of functionally novel BK-type currents that have yet to be identified in native cells.

Comparison of inactivation mediated by the β2 and β3 subunits

Inactivation of the BK channels mediated by the β2 subunit, although showing some features reminiscent of ball-and-chain inactivation of voltage-dependent K^+ channels (Hoshi et al., 1990), exhibits features suggesting that a different type of inacti-
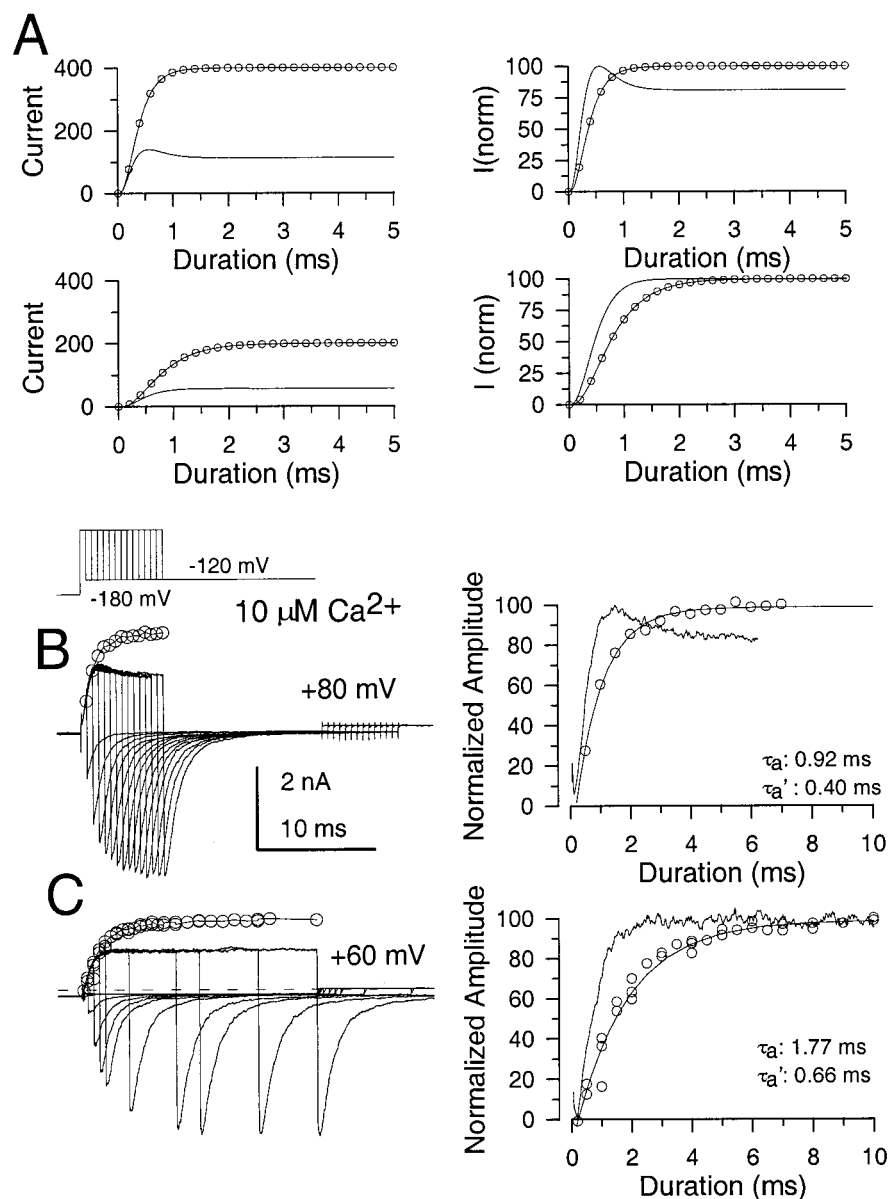
Figure 11. The rapid blockade results in current rectification and an increase in apparent current activation rate. *A*, Currents were simulated for Scheme I given in Materials and Methods (C1 ⇌ C2 ⇌ C3 ⇌ O ⇌ I). *Traces* on the *left* correspond to absolute currents in arbitrary units, with *open symbols* indicating *traces* for the same model when inactivation does not occur. For the *top panels*, a voltage of +40 mV was used, and for the *bottom panels*, the voltage was +20 mV. On the *right*, *traces* from the *left* were normalized to the same maximum amplitude to show the change in time-to-peak and apparent activation rate with rapid inactivation intact. *B*, β3 currents were activated with depolarizing steps to +80 with 10 μM Ca^{2+}. Repolarizing steps to −120 mV were applied at various times into the activation step to +80 mV. Tail current amplitudes exhibit a slower increase, even at a time when peak outward current exhibits slight inactivation. *Open circles* are the peak tail current amplitudes scaled to allow comparison of the relative conductances observed either at +80 mV or during the tail at −120 mV. The *open circles* emphasize the slow activation time course of the underlying channels and also the extensive rectification of conductance during the step to +80 mV. The *right panel* compares the normalized time course of outward current activation and the time course of the increase in tail current, with time constants given in the figure. *C*, Currents were activated by steps to +60 mV with 10 μM Ca^{2+}. Again, currents at +60 mV exhibit extensive rectification with no visible time-dependent inactivation. As shown in the *right panel*, the activation time course of outward current is faster than the time course of tail current development.

vation may be involved. In particular, cytosolic blockers of native inactivating BK channels or cloned β2 channels do not compete with the native inactivation domain (Solaro et al., 1997; Li et al., 1999; Xia et al., 1999), and furthermore, blocked channels do not recover through the open state to return to closed states (for native BK_i channels, Solaro et al., 1997; for α + β2 channels, C. J. Lingle, unpublished observations). It is possible that the β3 subunit might shed light on the β2 inactivation mechanism if the two shared similar features.

Both the β2 and β3 subunits produce inactivation mediated by trypsin-sensitive N-terminal domains of the subunits. β3 inactivation is much more rapid but incomplete, indicating that both the onset and recovery from inactivation mediated by the β3 subunit are more rapid. Like the β2 subunit, cytosolic blockers of the BK channel do not slow the β3 inactivation process. Qualitatively, we can only say that, in accordance with standard blocking models, neither the β2 nor β3 inactivation domain appears to bind to the mouth of the ion permeation pathway as defined by cytosolic blockers. This leaves open the possibility that both

inactivation domains act at the same site. Despite the kinetic differences, it also remains possible that both subunits act in the same way, only differing perhaps in the relative binding affinities of the inactivation domains.

Another unusual aspect of block produced by the β3 subunit was that, although recovery from block during repolarization to negative potentials was essentially instantaneous, we observed differences in the tail current time course after repolarization at the peak of outward current versus repolarization during steady-state block. We note here that this result (Fig. 6*B*), by itself, argues strictly against a simple block and unblocking of open channels. If all blocked channels recover very rapidly to the same open states, the tail currents should decay similarly. This is not observed. Rather, this phenomenon requires that during repolarization blocked channels recover to an open state that is different from that occupied by channels at the peak of outward current. Thus, inactivation mediated by both the β2 and β3 subunits exhibits features that are inconsistent with the behavior expected for simple, open channel block (Hoshi et al., 1990).

Rapid activation of BK current at moderate Ca^{2+}

An important property of current resulting from the β3 subunit is the relatively rapid current activation rate at low Ca^{2+}. How does this occur? By coupling a very rapid but partial blocking reaction with slow activation kinetics, the approach to steady-state after a step change in voltage reflects both the underlying activation rate and the inactivation rate. Rapid block, although producing marked current rectification, essentially decreases the rise time of the outward current by twofold to threefold over what it would be in the absence of the inactivation process. Because of this, an important role of the β3 subunit may be to increase effective current activation rates. Is a twofold to threefold increase in a current activation rate significant? As pointed out in Results, an increase in apparent rate of activation of this magnitude corresponds to an over 10-fold increase in effective $[Ca^{2+}]$ (Cui et al., 1997). The impact of this effect in a native cell would also critically depend on the density of channel expression.

Another unusual feature of the β3 variant is the more negative $V_{0.5}$ for activation than other variants (β1, β2) at $[Ca^{2+}]$ below 10 μM. In fact, the shift in $V_{0.5}$ produced by the β3 subunit relative to α alone appears to be relatively similar at all $[Ca^{2+}]$, whereas for β1 and β2 there appears to be larger effects at higher $[Ca^{2+}]$ (Wallner et al., 1996, 1999). This raises the possibility that the mechanism by which the β3 subunit affects apparent Ca^{2+} sensitivity may differ from the mechanism by which the β1 and β2 subunits may shift gating. As we noted above, the slowing of deactivation tail currents when channels close from the steady-state blocked condition indicates that channels can reside in more open states during the inactivated condition than during the peak of outward current. If the additional open states are, in fact, associated with the inactivation process itself, the occurrence of inactivation will increase the fraction of channels that appear in open states as monitored by the tail currents. This suggests that the blocking mechanism alone may account for much of the β3-induced shift in $V_{0.5}$ for observed at lower Ca^{2+}. Such a shift would be similar over all Ca^{2+}, because it would reflect exclusively the Ca^{2+}-independent equilibrium between open and blocked states.

If this hypothesis is correct, this would indicate that the inactivation mechanism of the β3 subunit has multiple physiologically important effects on the resulting BK current. Not only does the rapid blockade produce rectification, but it also increases the apparent current rise time and causes a shift in the $V_{0.5}$ of activation at low Ca^{2+}. It will be particularly interesting to determine how the remarkable properties conferred by this particular β3 variant are translated into Ca^{2+}-mediated regulation of cellular excitability in a real cell.

REFERENCES

Adelman JP, Shen KZ, Kavanaugh MP, Warren RA, Wu YN, Lagrutta A, Bond CT, North RA (1992) Calcium-activated potassium channels expressed from cloned complementary DNAs. Neuron 9:209–216.

Atkinson NS, Robertson GA, Ganetzky B (1991) A component of calcium-activated potassium channels encoded by the *Drosophila* slo locus. Science 253:551–555.

Brenner R, Jegla TJ, Wickenden A, Liu Y, Aldrich RW (2000) Cloning and functional characterization of novel large conductance calcium-activated potassium channel beta subunits, hKCNMB3 and hKC-NMB4. J Biol Chem 275:6453–6461.

Butler A, Tsunoda S, McCobb DP, Wei A, Salkoff L (1993) mSlo, a complex mouse gene encoding "maxi" calcium-activated potassium channels. Science 261:221–224.

Choi KL, Aldrich RW, Yellen G (1991) Tetraethylammonium blockade distinguishes two inactivation mechanisms in voltage-activated K^+ channels. Proc Natl Acad Sci USA 88:5092–5095.

Colquhoun D, Hawkes AG (1981) On the stochastic properties of single ion channels. Proc R Soc Lond B Biol Sci 211:205–235.

Cui J, Cox DH, Aldrich RW (1997) Intrinsic voltage dependence and Ca^{2+} regulation of mslo large conductance Ca-activated K^+ channels. J Gen Physiol 109:647–673.

Dworetzky SI, Boissard CG, Lum-Ragan JT, McKay MC, Post-Munson DJ, Trojnacki JT, Chang CP, Gribkoff VK (1996) Phenotypic alteration of a human BK (hSlo) channel by hSloβ subunit coexpression: changes in blocker sensitivity, activation/relaxation and inactivation kinetics, and protein kinase A modulation. J Neurosci 16:4543–4550.

Hamill OP, Marty A, Neher E, Sakmann B, Sigworth FJ (1981) Improved patch-clamp techniques for high-resolution current recording from cells and cell-free membrane patches. Pflügers Arch 391:85–100.

Hanner M, Schmalhofer WA, Munujos P, Knaus HG, Kaczorowski GJ, Garcia ML (1997) The beta subunit of the high-conductance calcium-activated potassium channel contributes to the high-affinity receptor for charybdotoxin. Proc Natl Acad Sci USA 94:2853–2858.

Hoshi T, Zagotta WN, Aldrich RW (1990) Biophysical and molecular mechanisms of Shaker potassium channel inactivation. Science 250:533–538.

Jones EM, Laus C, Fettiplace R (1998) Identification of Ca^{2+}-activated K^+ channel splice variants and their distribution in the turtle cochlea. Proc R Soc Lond B Biol Sci 265:685–692.

Knaus HG, Folander K, Garcia-Calvo M, Garcia ML, Kaczorowski GJ, Smith M, Swanson R (1994) Primary sequence and immunological characterization of beta-subunit of high conductance Ca^{2+}-activated K^+ channel from smooth muscle. J Biol Chem 269:17274–17278.

Lewin B (1997) Genes, Ch 30, pp 885–920. New York: Oxford UP.

Li ZW, Ding JP, Kalyanaraman V, Lingle CJ (1999) RINm5f cells express inactivating BK channels whereas HIT cells express noninactivating BK channels. J Neurophysiol 81:611–624.

McManus OB (1991) Calcium-activated potassium channels: regulation by calcium. J Bioenerg Biomembr 23:537–560.

McManus OB, Helms LM, Pallanck L, Ganetzky B, Swanson R, Leonard RJ (1995) Functional role of the beta subunit of high conductance calcium-activated potassium channels. Neuron 14:645–650.

Meera P, Wallner M, Toro L (2000) Molecular basis of charybdotoxin and iberiotoxin insensitive MaxiK channels: a novel β subunit. Biophys J 78:91.A.

Nimigean CM, Magleby KL (1999) The beta subunit increases the Ca^{2+} sensitivity of large conductance Ca^{2+}-activated potassium channels by retaining the gating in the bursting states. J Gen Physiol 113:425–440.

Oberst C, Weiskirchen R, Hartl M, Bister K (1997) Suppression in transformed avian fibroblasts of a gene (CO6) encoding a membrane protein related to mammalian potassium channel regulatory subunits. Oncogene 14:1109–1116.

Ramanathan K, Michael TH, Jiang GJ, Hiel H, Fuchs PA (1999) A molecular mechanism for electrical tuning of cochlear hair cells. Science 283:215–217.

Riazi MA, Brinkman-Mills P, Johnson A, Naylor SL, Minoshima S, Shimuizu N, Baldini A, McDermid HE (1999) Identification of a putative regulatory subunit of a calcium-activated potassium channel in the dup(3q) syndrome region and a related sequence on 22q11.2. Genomics 62:90–94.

Saito M, Nelson C, Salkoff L, Lingle CJ (1997) A cysteine-rich domain defined by a novel exon in a slo variant in rat adrenal chromaffin cells and PC12 cells. J Biol Chem 272:11710–11717.

Shen KZ, Lagrutta A, Davies NW, Standen NB, Adelman JP, North RA (1994) Tetraethylammonium block of Slowpoke calcium-activated potassium channels expressed in *Xenopus* oocytes: evidence for tetrameric channel formation. Pflügers Arch 426:440–445.

Solaro CR, Lingle CJ (1992) Trypsin-sensitive, rapid inactivation of a calcium-activated potassium channel. Science 257:1694–1698.

Solaro CR, Ding JP, Li ZW, Lingle CJ (1997) The cytosolic inactivation domains of BKi channels in rat chromaffin cells do not behave like simple, open-channel blockers. Biophys J 73:819–830.

Tseng-Crank J, Foster CD, Krause JD, Mertz R, Godinot N, DiChiara TJ, Reinhart PH (1994) Cloning, expression, and distribution of functionally distinct $Ca^{(2+)}$-activated K^+ channel isoforms from human brain. Neuron 13:1315–1330.

Tseng-Crank J, Godinot N, Johansen TE, Ahring PK, Strobaek D, Mertz

R, Foster CD, Olesen SP, Reinhart PH (1996) Cloning, expression, and distribution of a Ca$^{(2+)}$-activated K$^+$ channel beta-subunit from human brain. Proc Natl Acad Sci USA 93:9200–9205.

Uebele V, Wade T, Bennett P, Swanson R, Lagrutta A (2000) A novel family of alternatively spliced BK β-subunits. Biophys J 78:91.A.

Wallner M, Meera P, Ottolia M, Kaczorowski GJ, Latorre R, Garcia ML, Stefani E, Toro L (1995) Characterization of and modulation by a beta-subunit of a human maxi KCa channel cloned from myometrium. Receptors Channels 3:185–199.

Wallner M, Meera P, Toro L (1996) Determinant for beta-subunit regulation in high-conductance voltage-activated and Ca$^{(2+)}$-sensitive K$^+$ channels: an additional transmembrane region at the N terminus. Proc Natl Acad Sci USA 93:14922–14927.

Wallner M, Meera P, Toro L (1999) Molecular basis of fast inactivation in voltage and Ca^{2+}-activated K$^+$ channels: a transmembrane beta-subunit homolog. Proc Natl Acad Sci USA 96:4137–4142.

Wallner M, Meera P, Toro L (2000) Neuronal maxiK channel β subunit. Biophys J 78:91.A.

Wickenden A, Jegla T, Liu Y, Rigdon G (1999) A novel beta subunit of large conductance calcium-activated potassium channels that is highly expressed in brain. Soc Neurosci Abstr 25:2246.

Xia XM, Fakler B, Rivard A, Wayman G, Johnson-Pais T, Keen JE, Ishii T, Hirschberg B, Bond CT, Lutsenko S, Maylie J, Adelman JP (1998) Mechanism of calcium gating in small-conductance calcium-activated potassium channels. Nature 395:503–507.

Xia XM, Ding JP, Lingle CJ (1999) Molecular basis for the inactivation of Ca^{2+}- and voltage-dependent BK channels in adrenal chromaffin cells and rat insulinoma tumor cells. J Neurosci 19:5255–5264.